Particle production from String Percolation Model

Irais Bautista Guzmán

Seminario
FCFM -BUAP
17 de septiembre del 2014

Table of contents

Introduction
String Percolation Model

The multiplicity in pp and AA collisions
Rapidity dependence

Elliptic Flow
Azimuthal dependence Nuclear modification factor

Heavy flavor production

Conclusions

- String are supposed to describe confined QCD interactions in a effective way. They carry color charges at the ends and they extended their color field between the charges.
- They emit particles by string breaking and pair creation. $q\bar{q}$, $qq - \bar{q}\bar{q}$.
- In the proyecction on the impact parameter plane they look like disks of radius: $S_1 = \pi r_0^2$, $r_0 \sim 0.25$ fm.

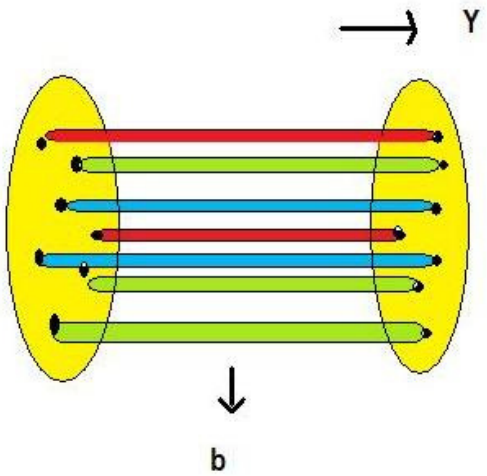

- The number of strings and the string density grows with energy and with the number of participating nucleons
- The number of strings grow and start to overlap forming clusters.
- At a critical density a macroscopic cluster appears and marks the percolation phase transition.
- Particles are produced by the Schwinger mechanisms.

- The formation of clusters behaves like disks in the continuum two dimensional percolation.
- $\eta^t = N_s \frac{S_1}{S_A}$
- For η^t larger than η_t^c a large cluster extend over the whole surface covering the fraction $1 - e^{-\eta_t}$ of the total area at which $(\eta_t = \eta_t^c)$ is approximately $2/3$. $\eta_c^t = 1.1 - 1.5$
- We assume a cluster of n strings behaves as a single string with higher color field, and momentum.
- $< \mu_n >= \sqrt{\frac{nS_n}{S_1}} < \mu_1 >, \;\; < p_{Tn}^2 >= \sqrt{\frac{nS_1}{S_n}} < p_{T1}^2 >$

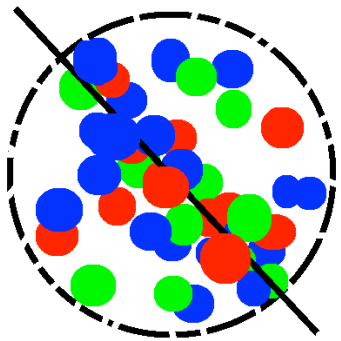

- In SPM the relevant quantity is the transverse impact parameter density η^t
- For pp collisions $\eta^t \equiv (\frac{r_0}{R_p})^2 \bar{N}_p^s$
- The particle density dn/dy at mid rapidity is related to the average number $\bar{N}_s$ of strings
  $\frac{dn}{dy} \sim F(\eta^t)\bar{N}_s$
  $F(\eta^t) = \sqrt{\frac{1-e^{-\eta^t}}{\eta^t}}$

The multiplicity distribution can be obtained from the cluster size distribution which approximately is a gamma function and the multiplicity distribution of the cluster, which is assume Poisson like in this way is obtained a negative binomial distribution.

$$P(n,s) = \frac{\Gamma(n+k)}{\frac{\Gamma(n+1)}{\gamma(k)}} \frac{\gamma^k}{(1+\gamma)^{n+k}}, \gamma = \frac{k}{< n >} \tag{1}$$

- The overlap area is given by $S_{N_A} = S_A(N_A/A)^\beta$, $\beta = 5/3$

$$N_A^s \simeq N_p^s N_A^{(\alpha+1)} \tag{2}$$

with

$$N_p^s = 2 + 4\left(\frac{r_0}{R_p}\right)^2 \left(\frac{\sqrt{s}}{m_p}\right)^{2\lambda}, \tag{3}$$

Notice that it would be expected

$$N_A^s \simeq N_p^s N_A^{4/3} \tag{4}$$

instead of

$$N_A^s = N_p^s N_A^{(\alpha+1)} \tag{5}$$

but the energy in pp is $\sqrt{s}$ and in AA is $A\sqrt{s}$, therefore at not very high energy some strings have not enough energy to be formed. The number should increase from A to $A^{4/3}$ with a $\ln s$ (phase space)

$$\eta_{N_A}^t = \eta_p^t N_A^{(\alpha(s))} \frac{A}{N_A^{2/3}} \tag{6}$$

- $$\left.\frac{1}{N_A}\frac{dn}{dy}\right|_{y=0} = \left.\frac{dn^{pp}}{dy}\right|_{y=0}\left(1+\frac{F(\eta^t_{N_A})}{F(\eta^t_p)}(N_A^{\alpha(\sqrt{s})}-1)\right), \quad (7)$$

- with
$$\alpha(s) = \frac{1}{3}(1-\frac{1}{1+ln(\sqrt{s/s_0}+1)}), \quad (8)$$
and
$$\left.\frac{dn^{pp}}{dy}\right|_{y=0} = \kappa\, F(\eta^t_p)\, N_p^s\,, \quad (9)$$

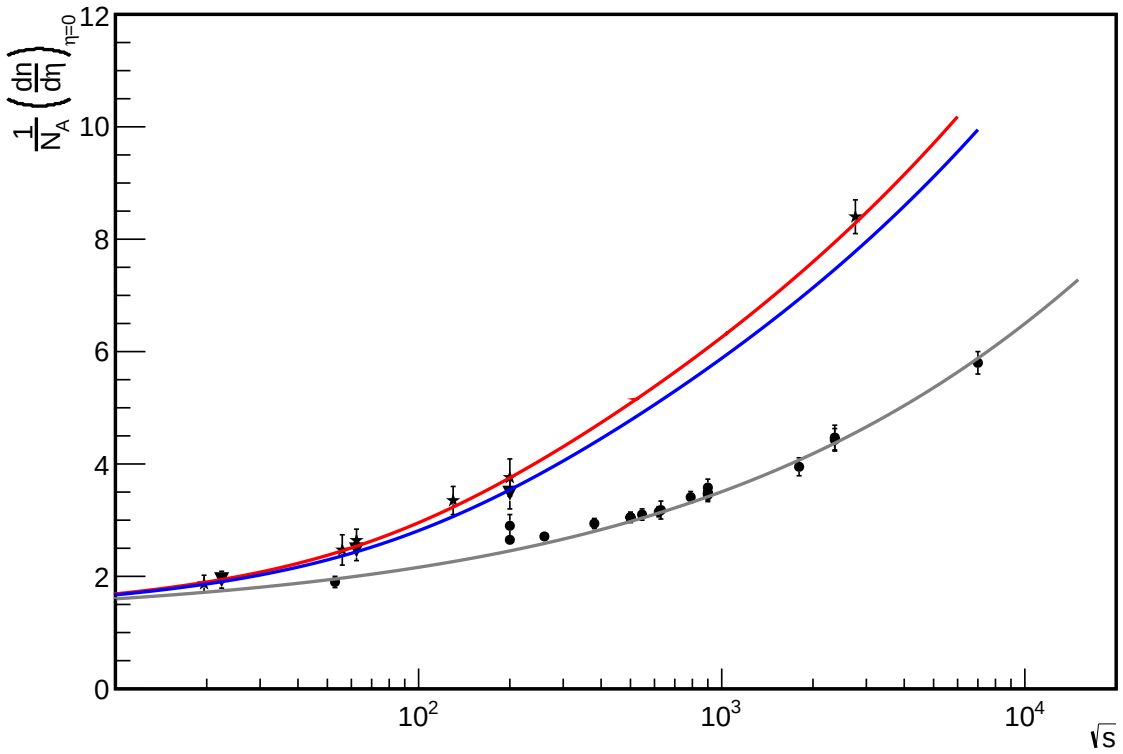

Figure: Multiplicity dependence on $\sqrt{s}$. Data from $p-p$, $Cu-Cu$, $Au-Au$ and $P-Pb$ is shown in circles, triangles and starts respectively. $(N_A = 1, A = 1)$ for is used for pp (grey line); $(NA = 50, A = 63)$ for CuCu (blue line); and $(NA = 175, A = 200)$ for AuAu/PbPb (red line)

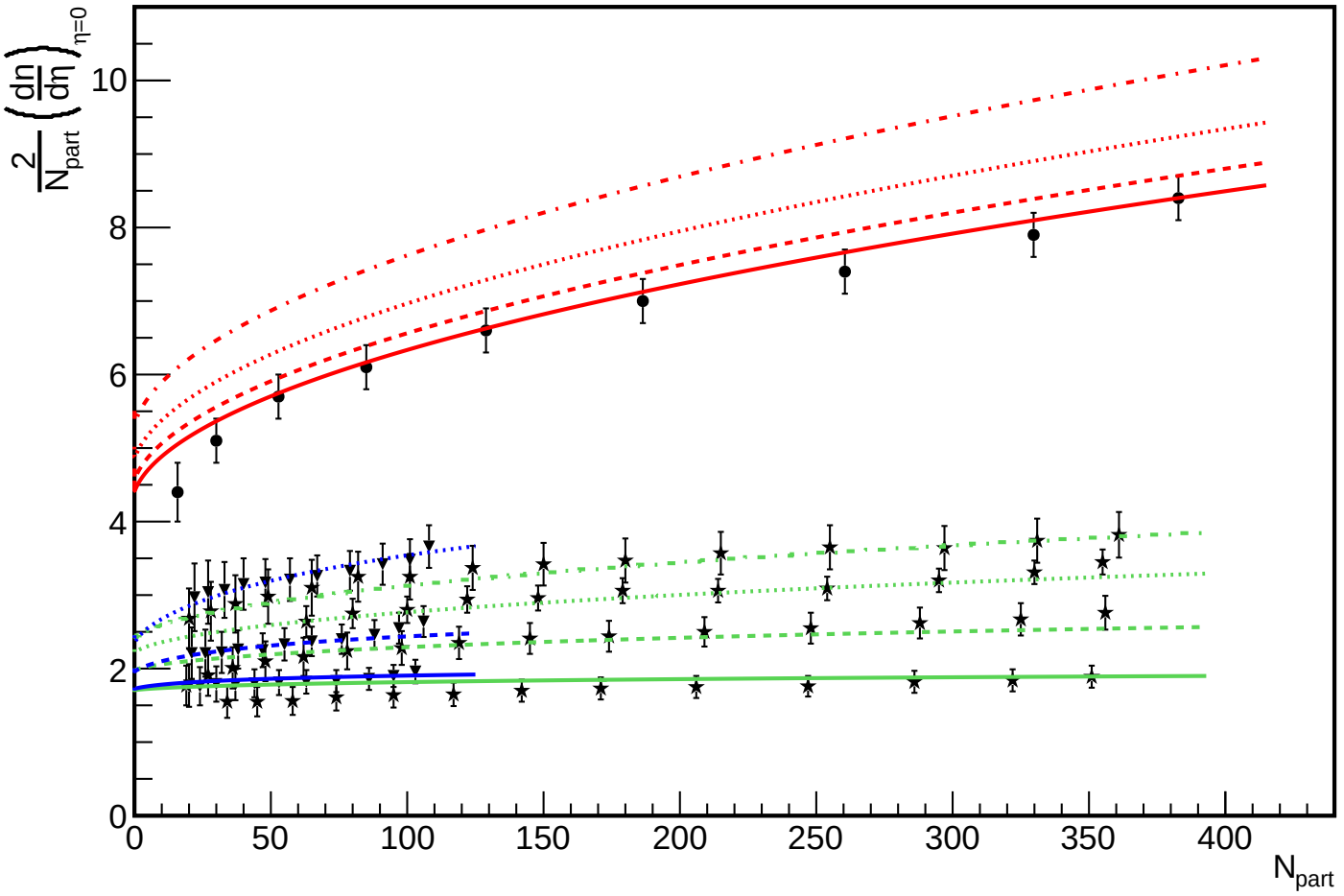
$\frac{2}{N_{part}}\left(\frac{dn}{d\eta}\right)_{\eta=0}$
0
2
4
6
8
10
0
50
100
150
200
250
300
350
400
N_{part}

$$\frac{dn}{dy} \sim F(\eta^t)\bar{N}_s, \tag{10}$$

with an exponential growth of the average number $\bar{N}_s$ of strings,

$$\bar{N}_s \sim e^{2\lambda Y}, \tag{11}$$

with $\lambda \simeq 0.2 - 0.3$, we write for the particle density, at $y \simeq 0$,

$$\frac{dn}{dy} \sim e^{\lambda Y}, \tag{12}$$

and for the full rapidity distribution,

$$\frac{dn}{dy}|_{pp} = ae^{\lambda Y}\frac{dn}{dy}|^s, \tag{13}$$

where $\frac{dn}{dy}|^s$ is the single string density, $\frac{dn}{d\eta}|_{pp}$

$$\frac{dn}{dy}|^s = \frac{1}{e^{\frac{\eta-(1-\alpha)Y}{\delta}}+1}, \tag{14}$$

$$\frac{dn}{d\eta}|_{pp} = J\frac{dn}{dy}|_{pp}, \tag{15}$$

with $J = \frac{cosh\eta}{\sqrt{k+sinh^2\eta}}$, $k = \frac{m^2+p_T^2}{p_T^2}$ and by assumption fix k at the effective value 1.2. It corresponds to $m_\pi \simeq 0.14$ GeV and $\bar{p}_\pi \simeq 0.3$ GeV.

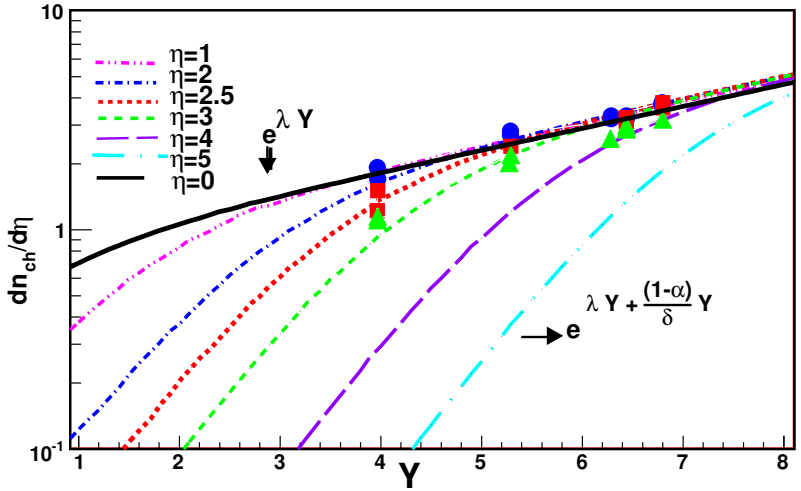

$$\frac{dn}{dn}(\eta \geq (1-\alpha)Y, Y) \sim e^{\lambda Y + \frac{(1-\alpha)}{\delta}Y} \tag{16}$$

$$\left.\frac{dn_{\rm ch}^{pp}}{d\eta}\right|_{\eta} = \kappa' J\, F(\eta_p^t)\, N_p^s \frac{1}{\exp\left(\frac{\eta-(1-\alpha)Y}{\delta}\right)+1} \qquad (17)$$

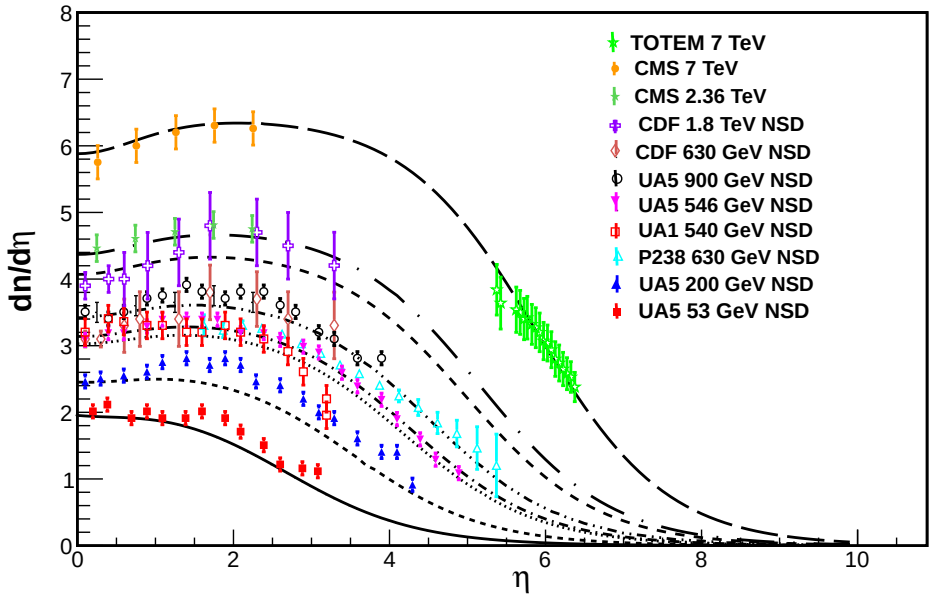

Comparison of the results from the evolution of the $\frac{dn_{ch}}{d\eta}$ with dependence in pseudorapidity for $p-p$ collisions at different energies (lines).

- Evolution in pseudorapidity for AA collisions

$$\frac{dn}{d\eta} = \kappa^{'} J(N_A) \frac{dn^{pp}}{dy}|_{y=0} \frac{(1 + \frac{F(\eta^t_{N_A})}{F(\eta^t_p)}(N_A^{\alpha(\sqrt{s})} - 1))}{\exp\left(\frac{-\eta-(1-\alpha)Y}{\delta}\right) + 1} \qquad (18)$$

with $\kappa' = \frac{\kappa}{J(\eta=0)}(\exp\left(\frac{-(1-\alpha)Y}{\delta}\right) + 1)$.

In all the computations we have used the following values of the parameters: $\kappa = 0.63 \pm 0.01$, $\lambda = 0.201 \pm 0.003$, $\sqrt{s_0} = 245 \pm 29$ GeV, $\alpha \simeq 0.34$, $\delta \simeq 0.84$ and $k_1 = 1.2$ to describe the particle density $\frac{dn}{d\eta}|_{N_A N_A}$ in the same power law as $\frac{dn}{d\eta}|_{pp}$. We had made here an extension to these descriptions to add the pseudo rapidity evolution.

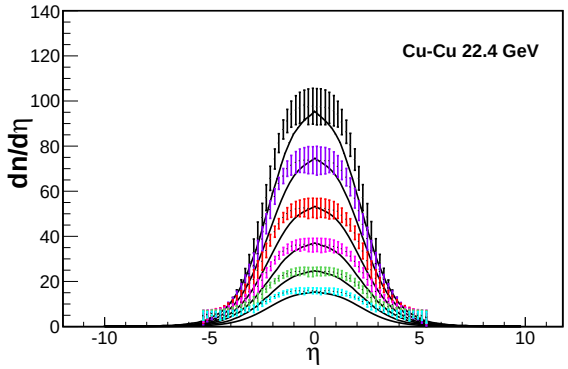

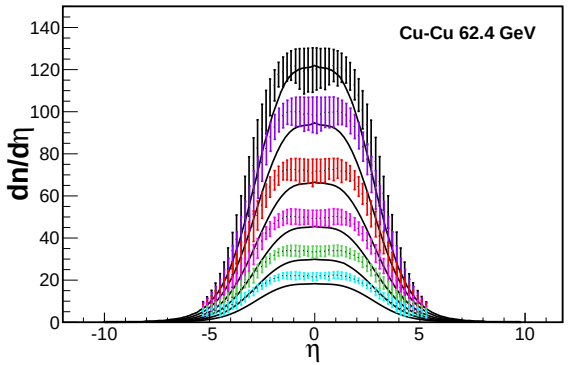

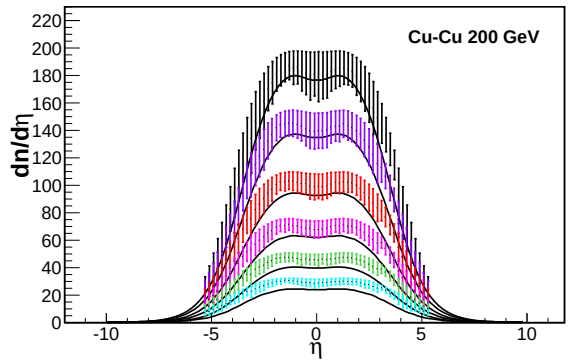

Figure: Evolution of the $dn_{ch}/d\eta$ with pseudorapidity for Cu-Cu collisions at 22.4 GeV, 62.4 GeV, and 200 GeV energies, data from ref. [1]. Error bars in color blue, green, pink, red, purple and black are used for the corresponding centralities $45-55\%$, $35-45\%$, $25-35\%$, $15-25\%$, $6-15\%$, $0-6\%$ respectively, black lines show our results.

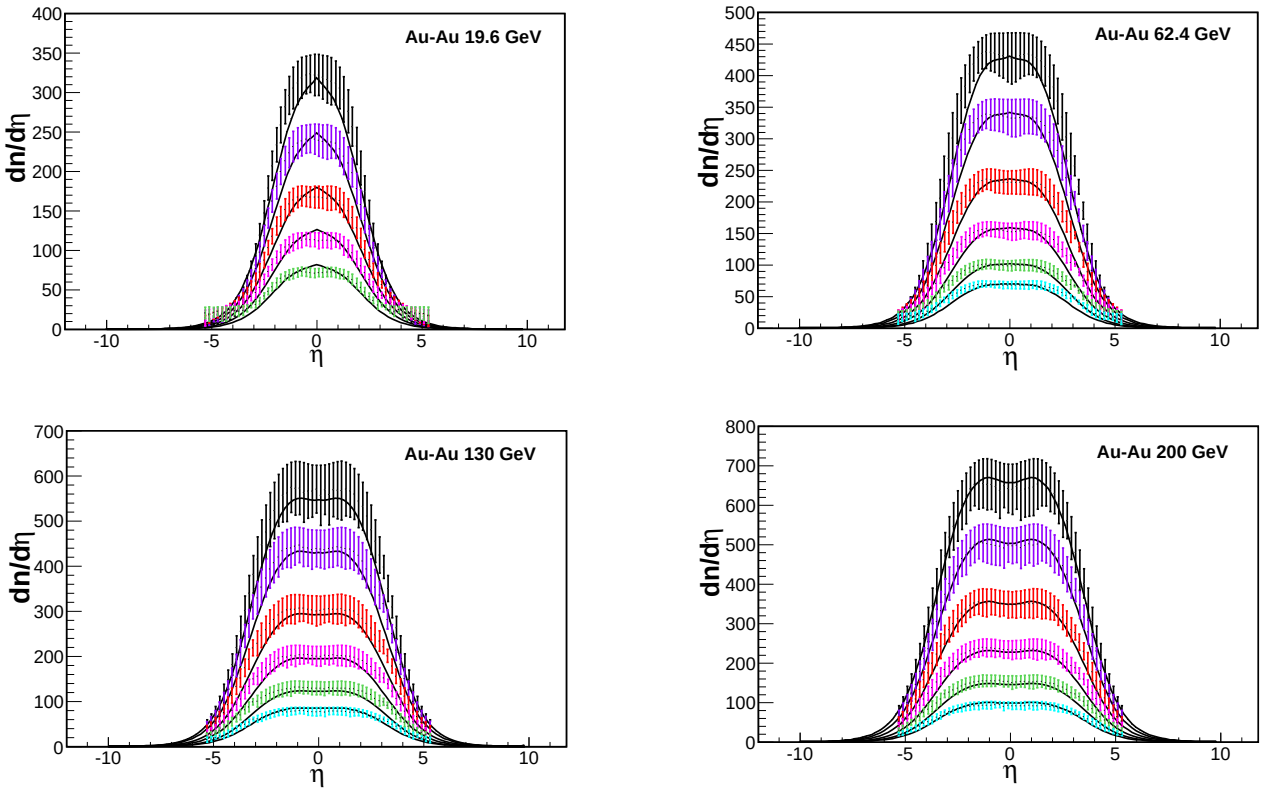

Figure: Evolution of the $dn_{ch}/d\eta$ with pseudorapidity for Au-Au collisions at 19.6 GeV, 62.4 GeV, 130 GeV and 200 GeV energies. Error bars in color blue, green, pink, red, purple and black are used for the corresponding centralities $45-55\%$, $35-45\%$, $25-35\%$, $15-25\%$, $6-15\%$, $0-6\%$ respectively, black lines are the model results.

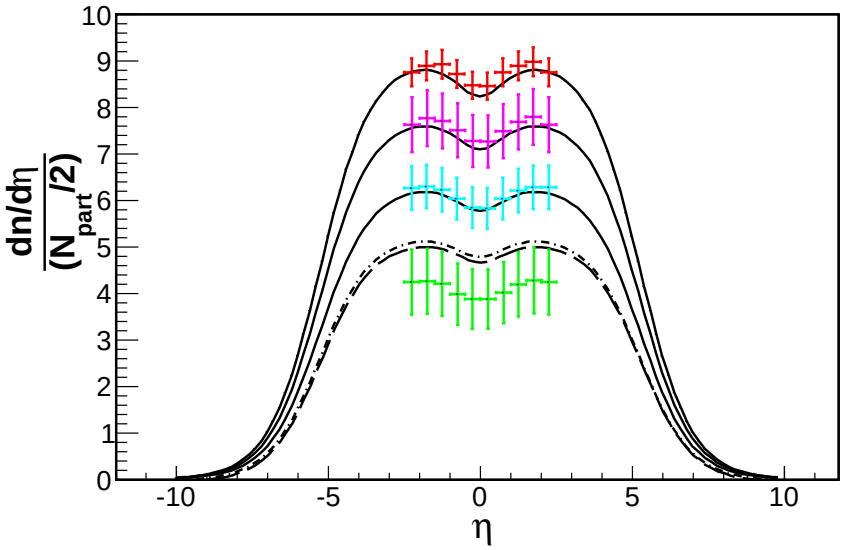

Figure: Comparison of the results from the evolution of the $\frac{dn_{ch}}{d\eta}\frac{1}{(N_{part}/2)}$ with the pseudorapidity for Pb-Pb collisions at 2.76 TeV. Error bars in color green, blue, pink and red are used for the corresponding centralities $85-95\%$, $50-55\%$, $0-90\%$ and $0-5\%$ respectively, lines in black are the corresponding results from the model to the respective centrality, for the smaller centrality we use the number of participants corresponding to the 85-95% showed in dot and dashed line and in dashed line is the minimum number of participants equal 2.

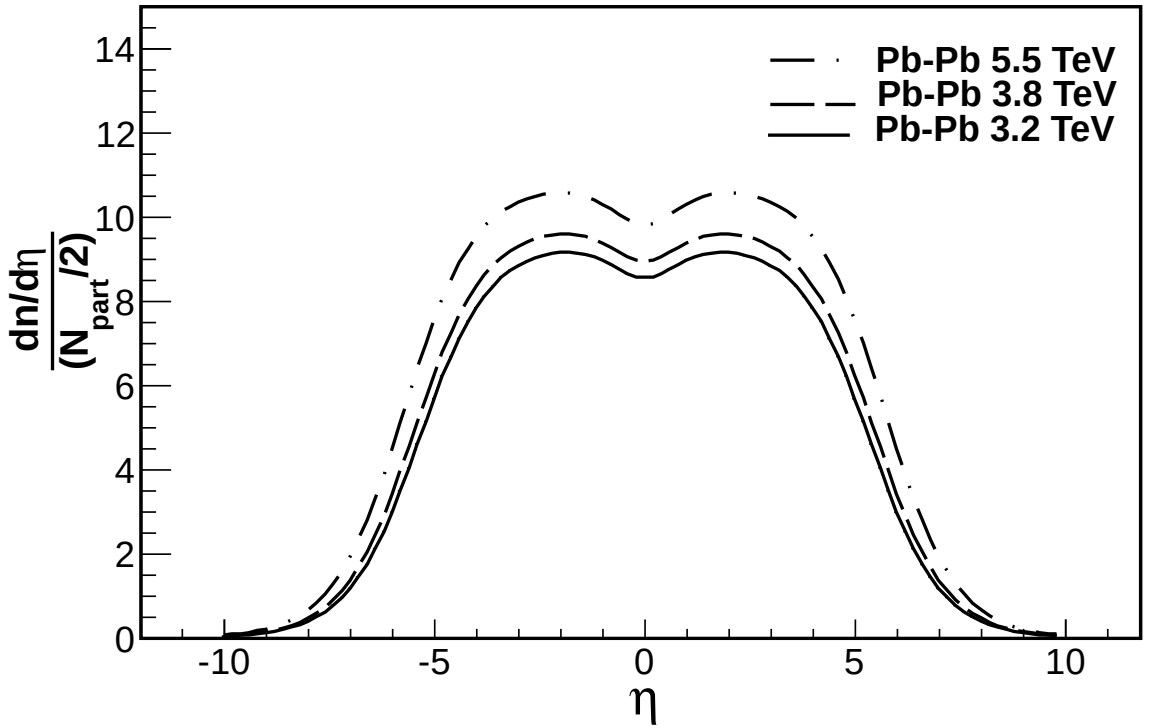

Figure: Predictions on the evolution of the $\frac{dn_{ch}}{d\eta}\frac{1}{(N_{part}/2)}$ with pseudorapidity for Pb-Pb collisions at 3.2, 3.9 and 5.5 TeV energies at $0-5\%$ centrality.

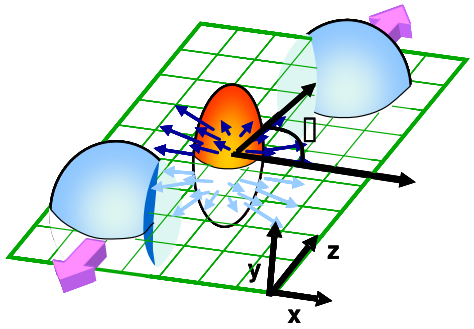

- A convenient way of characterizing the various patterns of anisotropic flow is to use a Fourier expansion of the invariant triple differential distributions,

$$v_n(p_T, y) =< cos[n(\varphi - \Psi_{RP}] >, \tag{19}$$

$$E\frac{d^3N}{d^3p} = \frac{1}{2\pi}\frac{d^3N}{p_T dp_y p_y}(1 + 2\Sigma_{n=1}^{\infty} v_n cos[n(\varphi - \Psi_{RP})]) \tag{20}$$

- One can write the transverse momentum distribution as

$$f(p_T, y) = \frac{dN}{dp_T^2 dy} = \int_0^\infty dx W(x) f(p_T, x)$$

$$= \frac{dN}{dy} \frac{k-1}{k} \frac{1}{<p_{T1}^2>_i} F(\eta^t) \frac{1}{(1+\frac{F(\eta^t)p_T^2}{k<p_T^2>_i})^k}$$

$\mu_{\bar{B}} = N_s^{1+\alpha} F(\eta_{\bar{B}}^t) \mu_{1\bar{B}}$

- Where $\alpha = 0.09$ and $\mu_{1\bar{B}} \sim 0.033 \mu_{1\pi}$.
- This means that η^t must be replaced by $\eta_{\bar{B}} = N_s^\alpha \eta^t$.

$$\frac{\pi R^2}{4} = \frac{1}{2}\int_0^{\frac{\pi}{2}} R_\varphi^2 d\varphi \tag{21}$$

and

$$R^2 = < R_\varphi^2 > \tag{22}$$

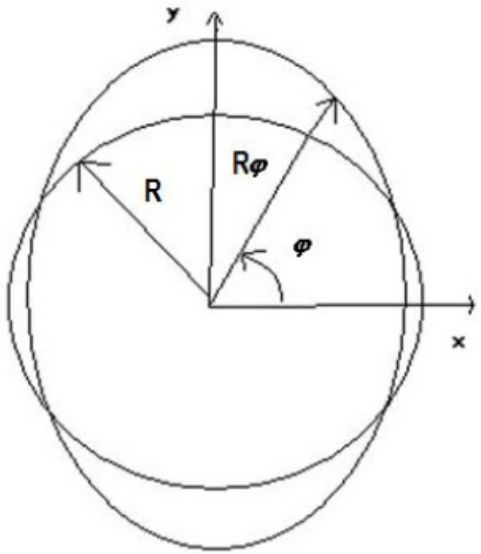

$$\frac{dn}{dy\ dp_t^2\ d\varphi}\ |_{y=0} \equiv f\left(p_t^2, R_\varphi^2\right) \tag{23}$$

$$\frac{dn}{dy\ dp_t^2}|_{y=0} \equiv f\left(p_t^2, R^2\right). \tag{24}$$

$$f\left(p_t^2, R_\varphi^2\right) \simeq \frac{2}{\pi} f\left(p_t^2, R^2\right)\left[1 + \frac{\partial \ln f\left(p_t^2, R^2\right)}{\partial R^2}\left(R_\varphi^2 - R^2\right)\right]. \tag{25}$$

$$\int_0^{\pi/2} f\left(p_t^2, R_\varphi^2\right) d\varphi = f\left(p_t^2, R^2\right) \tag{26}$$

$$\frac{\partial f\left(p_t^2, R^2\right)}{\partial R^2} < 0. \tag{27}$$

- The expression for the elliptic flow.

$$v_2\left(p_T^2\right) = \frac{2}{\pi}\int_0^{\frac{\pi}{2}} d\varphi\, cos(2\varphi)\left[1 + \frac{\partial \ln f_{AA}\left(p_t^2, R^2\right)}{\partial R^2}\left(R_\varphi^2 - R^2\right)\right] \tag{28}$$

$$= \frac{2}{\pi}\int_0^{\pi/2} d\varphi cos2\varphi\left(\frac{R_\varphi}{R}\right)^2\left(\frac{e^{-\eta^t} - F(\eta^t)^2}{2F(\eta^t)^2}\right)\frac{F(\eta^t)p_T^2/<p_T^2>_1}{(1+F(\eta^t)p_T^2/<p_T^2>_1)}.$$

- The normalized values used in calculations: $< p_T^2 >_{1p}= 0.30$ GeV/c, $< p_T^2 >_{1k}= 0.14$ GeV/c, $< p_T^2 >_{1\pi}= 0.060$ GeV/c,

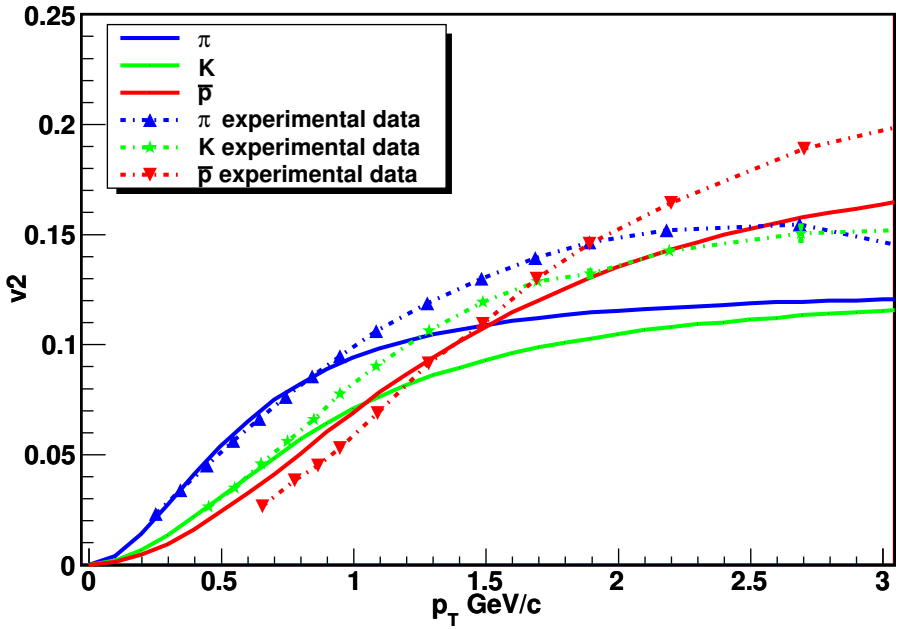

Figure: Elliptic flow for different hadron species, comparison between our results and experimental data from RHIC in Au+Au collisions.

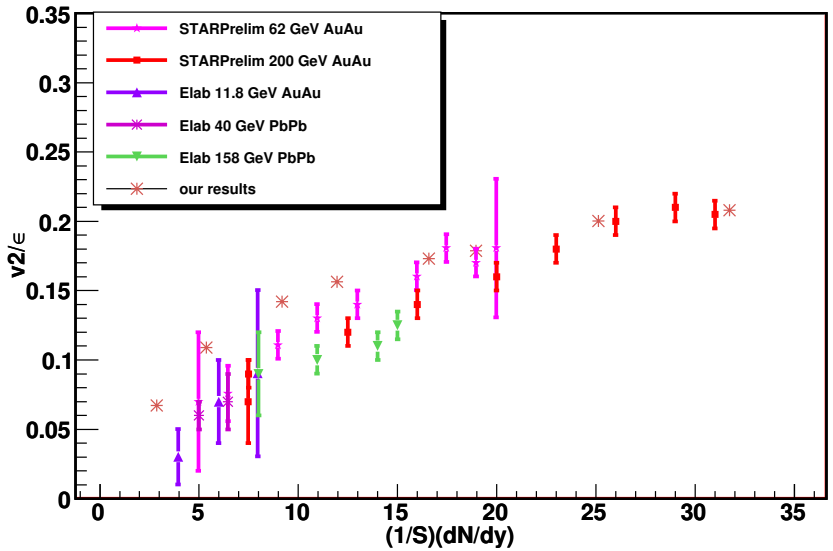
STARPrelim 62 GeV AuAu
STARPrelim 200 GeV AuAu
Elab 11.8 GeV AuAu
Elab 40 GeV PbPb
Elab 158 GeV PbPb
our results
v2/ϵ
(1/S)(dN/dy)
0.35
0.3
0.25
0.2
0.15
0.1
0.05
0
0
5
10
15
20
25
30
35

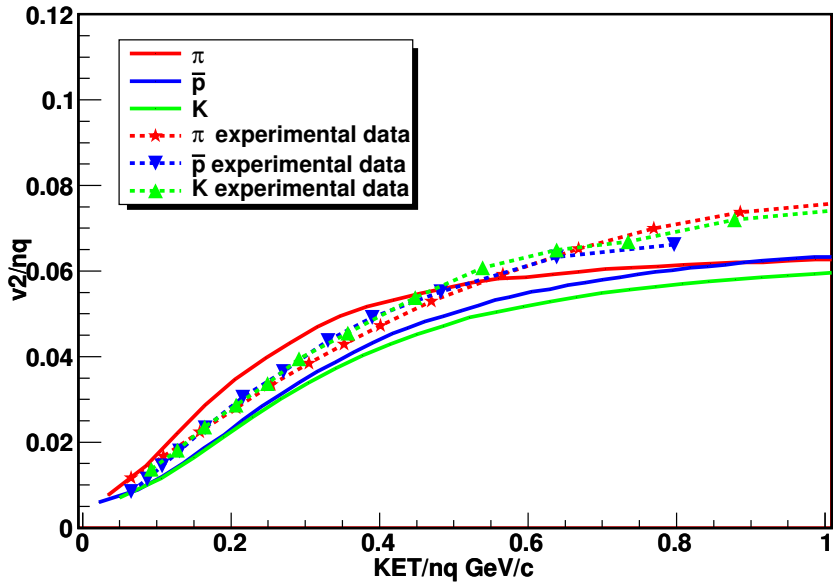
0.12
0.1
0.08
0.06
0.04
0.02
0
v2/nq
0
0.2
0.4
0.6
0.8
1
KET/nq GeV/c
π
p̄
K
π experimental data
p̄ experimental data
K experimental data

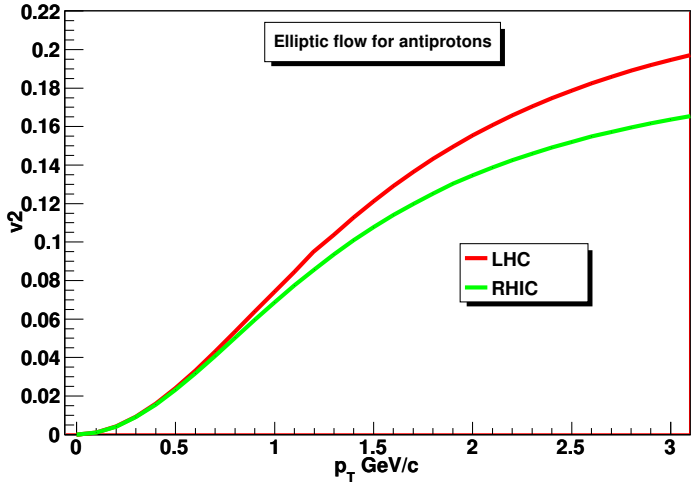
Elliptic flow for antiprotons
LHC
RHIC
v2
p_T GeV/c

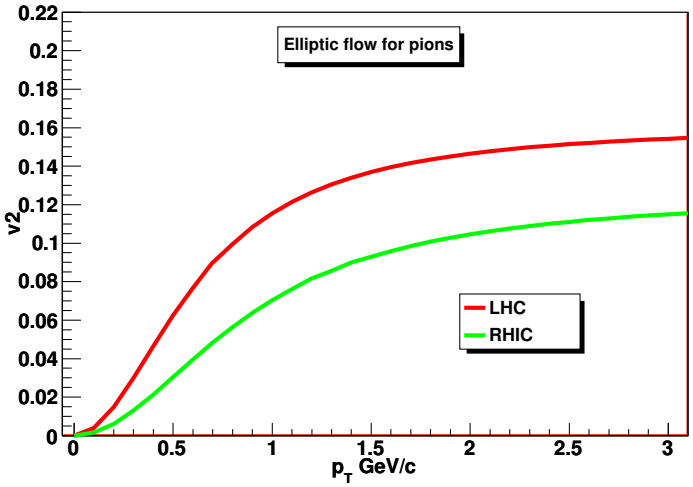
Elliptic flow for pions
LHC
RHIC
v2
p_T GeV/c

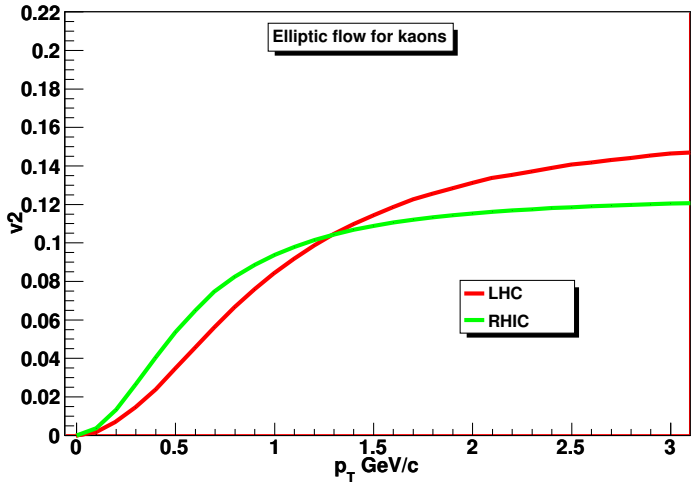
Elliptic flow for kaons
LHC
RHIC
v2
p_T GeV/c

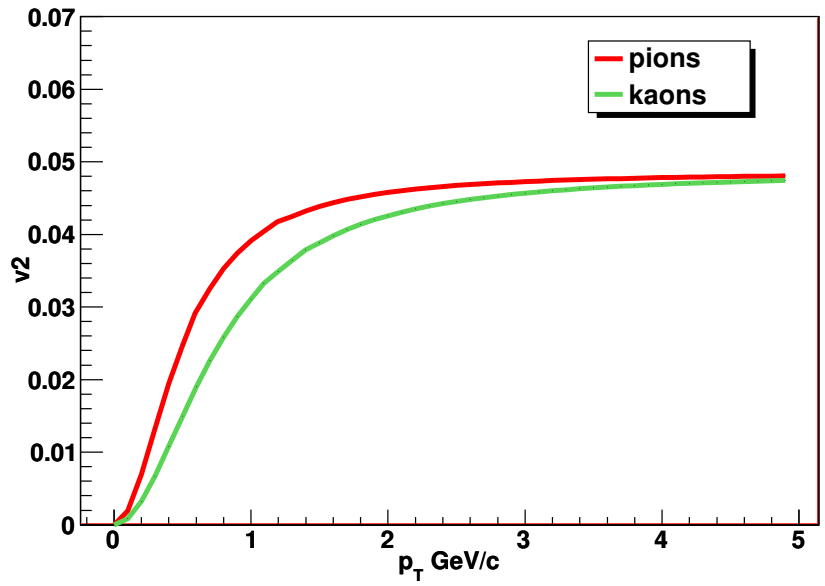
pions
kaons
v2
0.07
0.06
0.05
0.04
0.03
0.02
0.01
0
0
1
2
3
4
5
p_T GeV/c

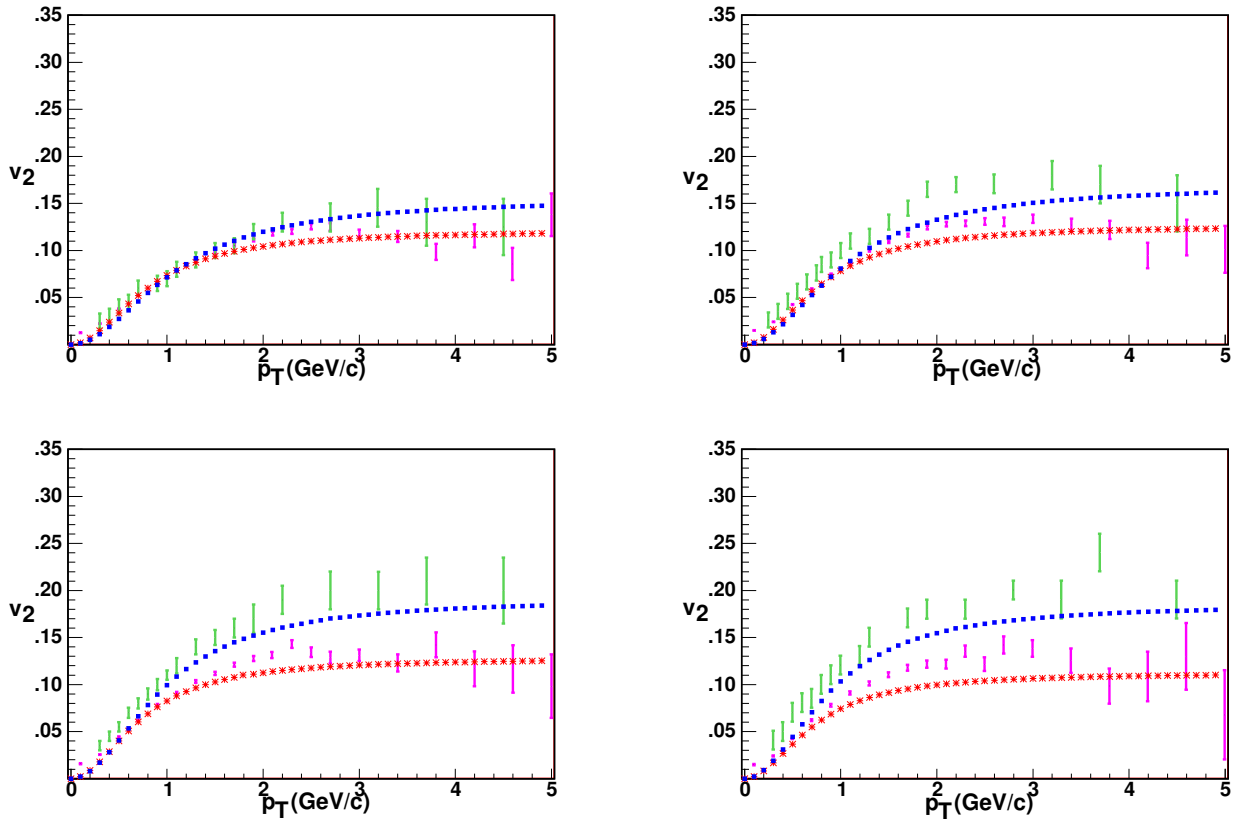

Figure: Predictions for $\sqrt{s} = 200$ GeV and $\sqrt{s} = 2.76$ TeV energies, and error-bars in green and pink are the respective data for centralities $10 - 20\%$, $20 - 30\%$, $30 - 40\%$, $40 - 50\%$ repectively

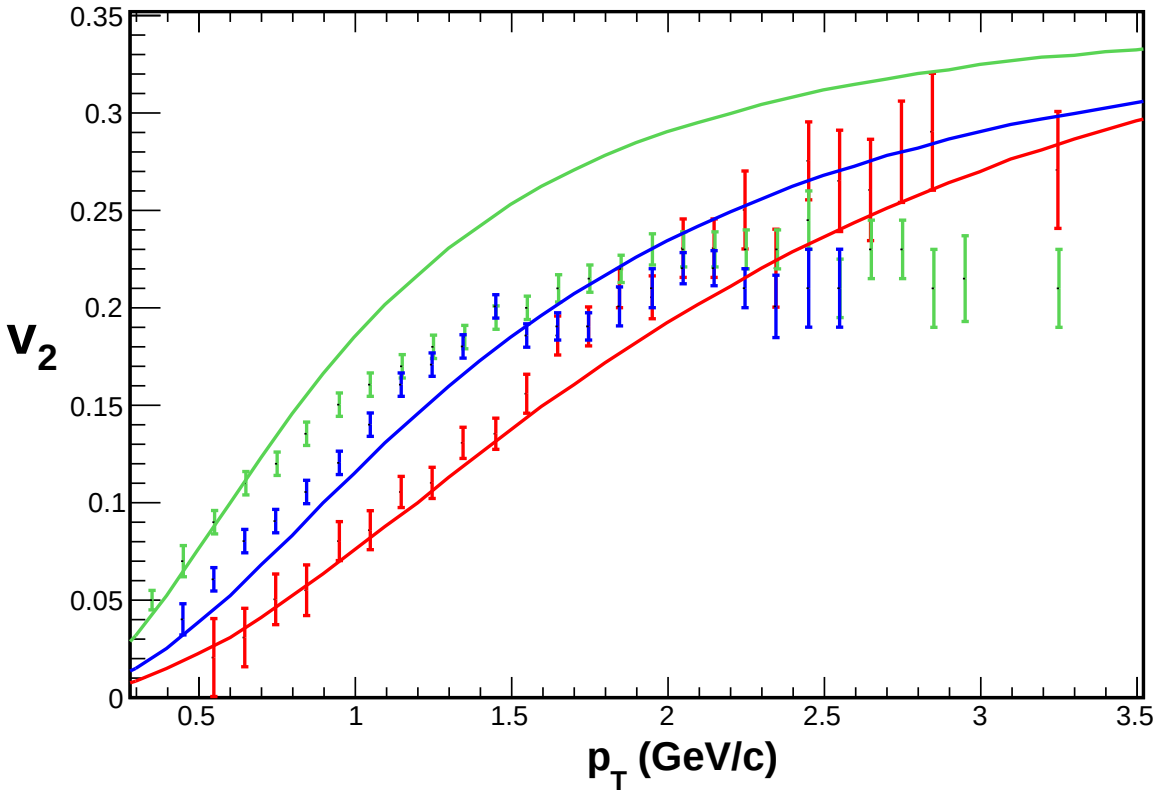

Figure: Solid lines, in red, green and blue corresponds to the proton, kaon, and pion predictions for central $Pb - Pb$ collisions respectively at $\sqrt{s} = 2.76$ TeV.

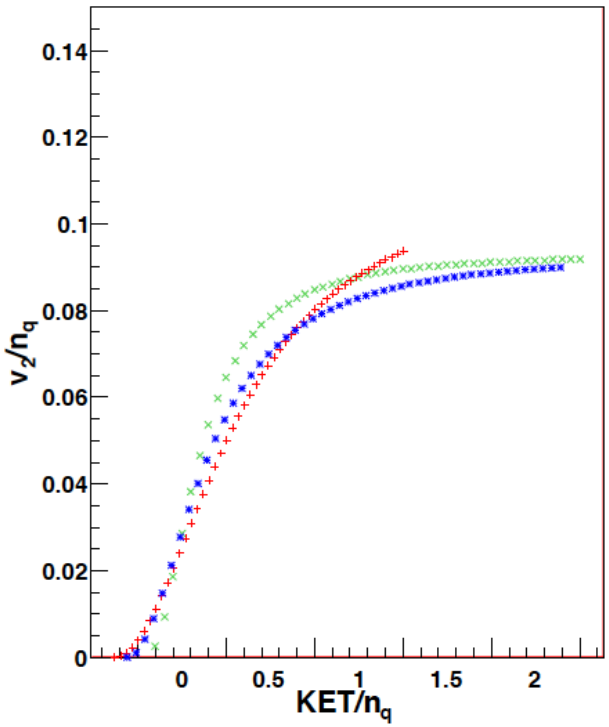

Figure: Elliptic flow scaling with the number of quark constituents for central $Pb - Pb$ collisions at $\sqrt{s} = 2.76$ TeV. Symbols $(+)$ in red,$(*)$ in blue and (x) in green are used for protons kaons and pions respectively.

- $$R_{AA} = \frac{\frac{d\sigma^{AA\to h}}{dyd^2p_T}}{N_{coll}\frac{d\sigma^{pp\to h}}{dyd^2p_T}}, \tag{29}$$

$$R_{AA}(p_t^2, \Delta\varphi) \equiv \Delta\varphi \frac{f_{AA}(p_t^2, R_\varphi^2)}{\langle N_{coll.}\rangle f_{pp}(p_t^2, R'^2)}$$

$$= \Delta\varphi R_{AA}(p_t^2)\left[1 + \frac{\partial \ln f_{AA}(p_t^2, R^2)}{\partial R^2}\left(R_\varphi^2 - R^2\right)\right] \tag{30}$$

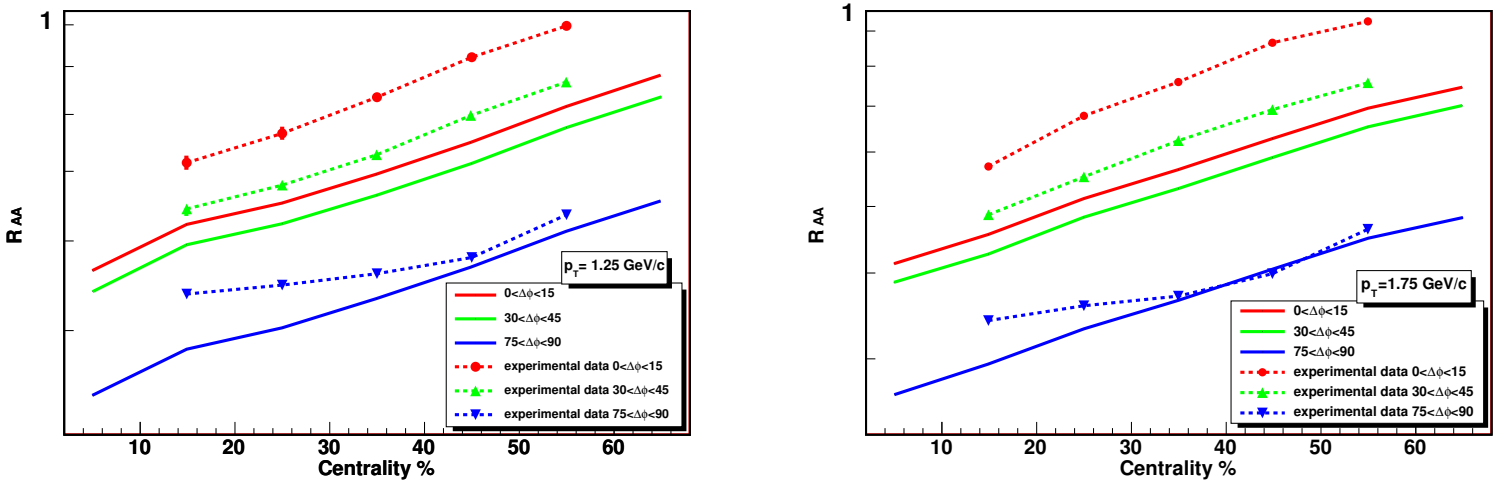

Figure: Angular suppression for pions for $p_T = 1.25$, $p_T = 1.75$GeV/c at different centrality, $(10-20\%, 20-30\%, 30-40\%, 50-60\%)$ results compared to PHENIX data.

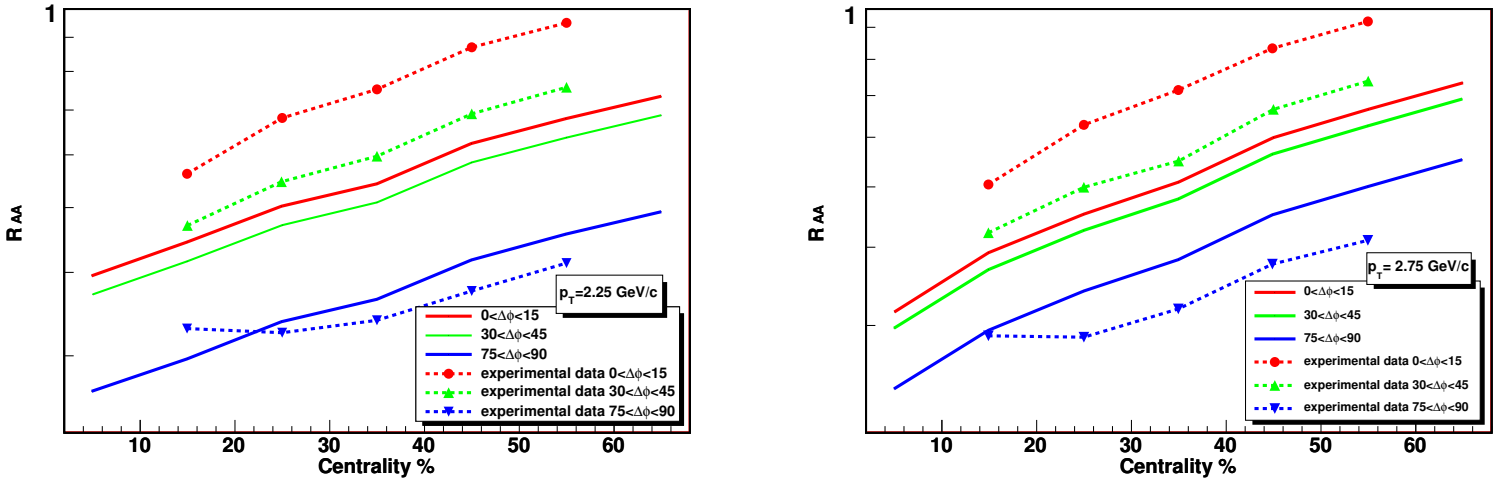

Figure: Angular suppression for pions for $p_T = 2.25$, $p_T = 2.75$GeV/c at different centrality, $(10-20\%, 20-30\%, 30-40\%, 50-60\%)$ results compared to PHENIX data.

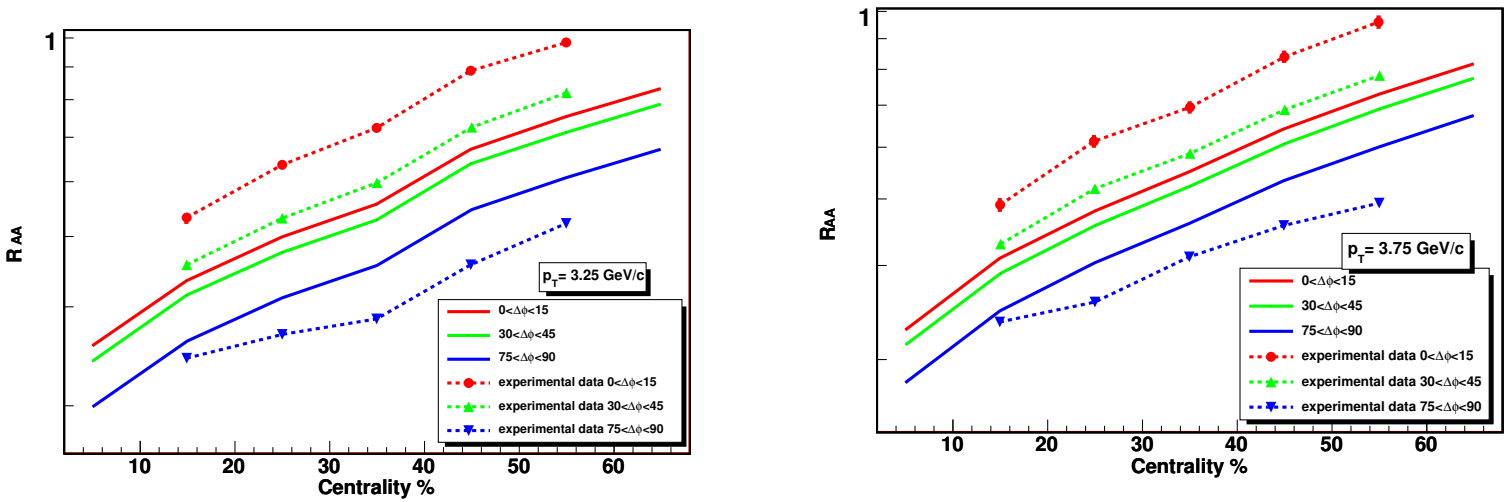

Figure: Angular suppression for pions for $p_T = 3.25$, $p_T = 3.75$ GeV/c at different centrality, $(10 - 20\%, 20 - 30\%, 30 - 40\%, 50 - 60\%)$ results compared to PHENIX data.

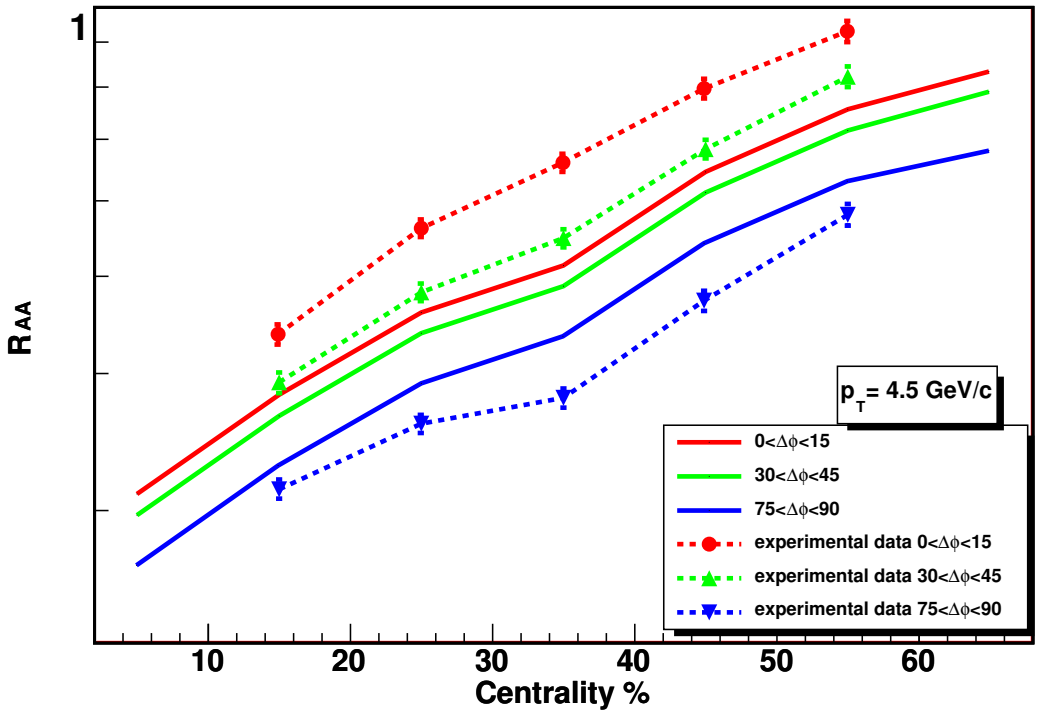

Figure: Angular suppression for pions for $p_T = 4.5$ GeV/c at different centrality, $(10-20\%, 20-30\%, 30-40\%, 50-60\%)$ results compared to PHENIX data.

- the single non- photonic nuclear modified factor, R^e_{AA} can be expressed as $R^e_{AA} = R^{D+\Lambda}_{AA} F$ where $R^{D+\Lambda}_{AA}$ is the nuclear modified factor for D and Λ_c, i.e.

$$R^{D+\Lambda}_{AA} = \frac{N^D_{AA} + N^\Lambda_{AA}}{N_{coll}(N^D_{pp} + N^\Lambda_{pp})} \tag{31}$$

being N^D and N^Λ the produced D and Λ in AA or pp collisions and the N_{coll} is the number of collisions at a given centrality. The factor, F, is given by the expression

$$F = \frac{(1+a)(1+xCa)}{(1+Ca)(1+xa)}, \tag{32}$$

- being, a, and, Ca, the charmed baryon to meson ratio in proton-proton and A-A collisions respectively. Therefore, C, represents the enhancement factor for the ratio of charm baryons to mesons in AA as compared to pp collisions. Here x is the ratio between the branching ratios for the inclusive decay of Λ and D into electrons.
- $a = (\frac{\Lambda}{D})_{pp}$, $Ca = (\frac{\Lambda}{D})_{AA}$, $x = \frac{B^{\Lambda \to e}}{B^{D \to e}}$

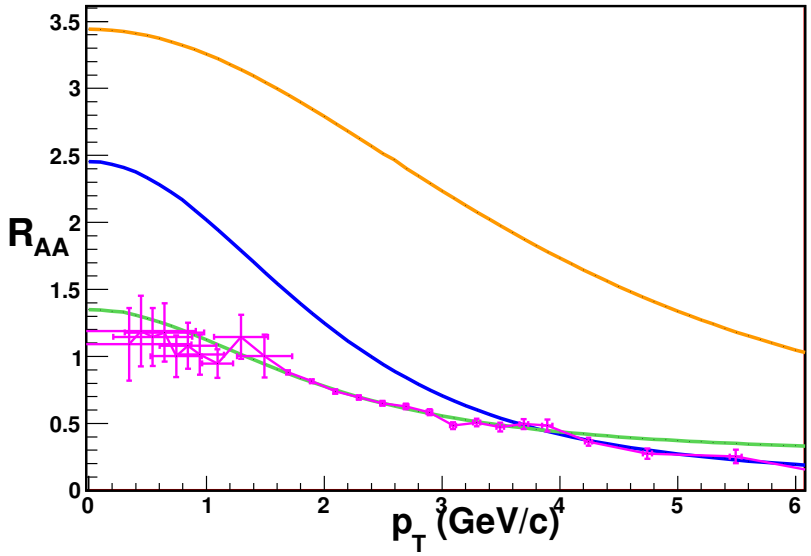

Figure: R_{AA} Λ_c (blue), D^0 (green) and B^0 (orange) for Au+Au central collisions data from PHENIX.

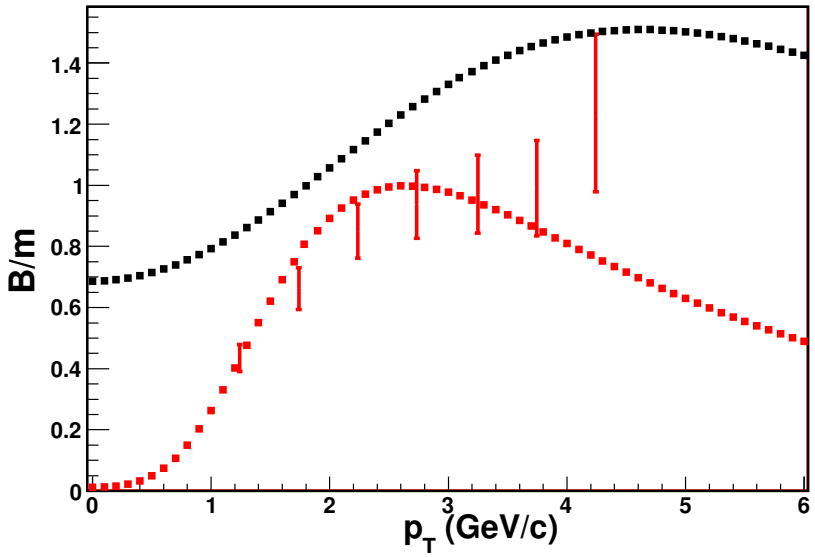

Figure: Ratio Λ_c/D^0 in black, and $\bar{p}/\pi$ in red, for Au-Au central collisions at $\sqrt{s} = 200$ (GeV/c), data from PHENIX.

- There is a non-linear dependence of $\frac{1}{N_A} dn/d\eta|_{AA}$ on $dn/d\eta|_{pp}$.
- Particle densities, as a function of η and Y give a good description of Pb-Pb data at LHC in a wide region in η. The same is observed for pp in a wide range of rapidity Y.
- The multiplicity dependence of N_A in AA collisions is shown to be well described by the string percolation model for different nuclei species.
- In the study the evolution of the particle density, $dn/d\eta$ at fixed η, with the beam rapidity Y its been shown that the width of the plateau increases proportionally to Y, and that the particle density, reduces to a step function in the limit that Y goes to infinity.

- The evolution of the multiplicity dependence on the rapidity at different energy does not show limit fragmentation.
- The comparison of the elliptic flow with RHIC experimental data for $p_T < 1.5$ GeV/c shows a reasonable agreement. In particular, the observed mass ordering is reproduced.
- Its been shown that the elliptic flow in SPM indicates that above a determined density elliptical flow decreases slowly.
- A sizable elliptic flow in proton proton collisions has been predicted as a consequence of the high partonic density reached at LHC energy.
- The reasonable agreement obtained in SPM with the experimental data for $p_T < 1.5$ GeV/c, confirms the common belief that elliptic flow reveals a strongly interacting medium created in the first stage of the collision.

- The transverse momentum dependence of v_2 and its values are very similar at RHIC and LHC energies for all centralities, in agreement with the experimental data. The integrated elliptic flow at mid rapidity is around 25% higher at $\sqrt{s} = 2.76$ TeV than at $\sqrt{s} = 200$ GeV and in the rapidity dependence of the elliptic flow there is no longer a triangle shape shown at RHIC.
- The result on the elliptic flown give a consistent picture with the formation of a fluid with a low ratio between shear viscosity and entropy in the range of energies of RHIC and LHC.
- We have computed the dependence of the nuclear modify factor on the azimuthal angle comparing our results with experimental data for different centralities. We reproduce the general trend of the data, although we are 15% below for small angles.

- We had evaluate the nuclear modification factor for D_0,Λ_c and B at RHIC energies, computing also the baryon to meson ratio in AA and pp collisions.
- The overlapping of the strings formed in the collision of heavy nuclei particles produces strong color fields which give rise to an enhancement of heavy flavour.

Thank you...

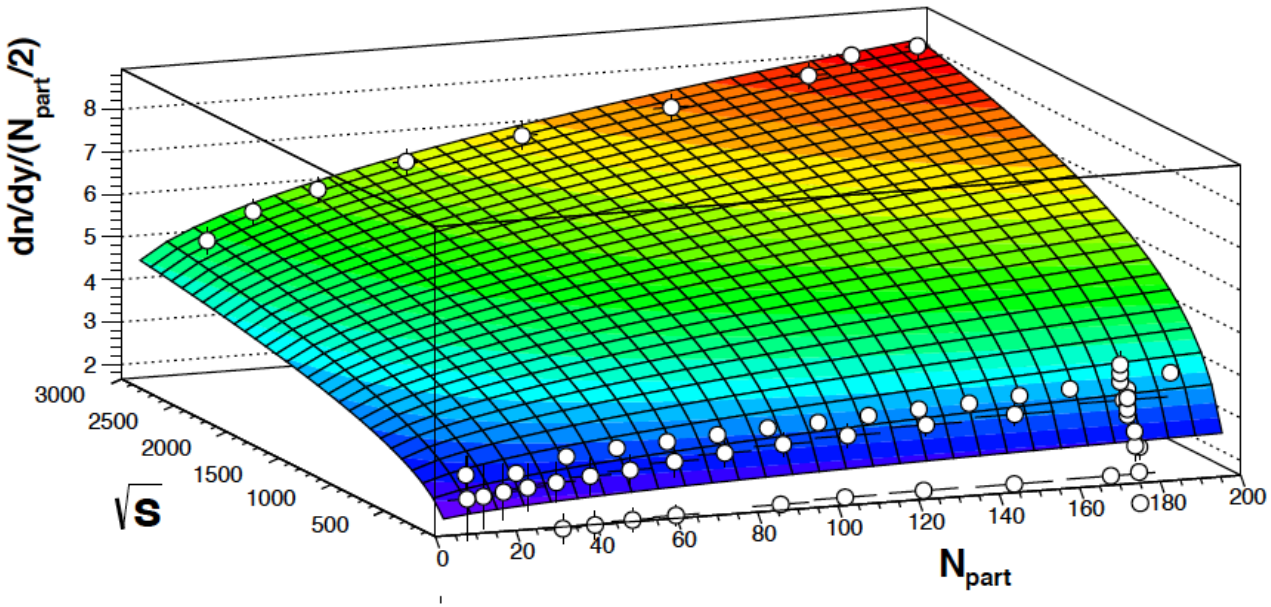
dn/dy/(N_part/2)
8
7
6
5
4
3
2
3000
2500
2000
1500
1000
500
√s
0
20
40
60
80
100
120
140
160
180
200
N_part

- What is the smallest (in terms of size and energy content) droplet of QGP to which a fluid dynamical description can be applied?
- When one selects high multiplicity final states in p/dA collisions or pp collisions, what features of the initial state or of the subsequent dynamics are being selected? If by selecting high multiplicity final states one is selecting collisions in which droplets of QGP are formed, how large are the protons in the initial states of the selected collisions? And, how large are the droplets of QGP that are formed?
- Is the observed collectivity in momentum space driven by the spatial structure (i.e. the pressure gradients) of the initial matter distribution created in the collision, as assumed by current hydrodynamic models?
- Is there a common way to calculate the initial conditions from first principles?

- Are there mechanisms other than hydrodynamics that can generate and quantitatively reproduce the observed collective features in these collisions?
- How does collectivity emerge as a function of system size and energy density?
- What are the relevant scales (time, energy, size) controlling the degree of collectivity observed in the final state?
- To which extent can a collective effect observed in a larger system be reduced to a superposition of more elementary collisions? Can this experimentally be studied by selecting events in which properties of either the smaller system or new collective effects are enhanced?

- How can we use our ability to probe different collision energies, centralities and other event characteristics and to vary the size and shape of the colliding nuclei to shed light on the mechanisms that drive the emergence of the apparent collective behavior in high-energy collisions?
- How is the onset of collective bulk dynamics in small systems correlated with hard probes of the medium?

References from this talk can be found in

I. Bautista, C. Pajares, J. G. Milhano and J. Dias de Deus, Phys. Rev. C **86** (2012) 034909 [arXiv:1206.6737 [nucl-th]].

I. Bautista, J. G. Milhano, C. Pajares and J. Dias de Deus, Phys. Lett. B **715** (2012) 230 [arXiv:1204.1457 [nucl-th]].

I. Bautista, L. Cunqueiro, J. D. de Deus and C. Pajares, J. Phys. G **37** (2010) 015103 [arXiv:0905.3058 [hep-ph]].

I. Bautista and C. Pajares, Phys. Rev. C **82** (2010) 034912 [arXiv:1009.5843 [hep-ph]].

I. Bautista, C. Pajares and J. D. de Deus, Nucl. Phys. A **882** (2012) 44 [arXiv:1110.4740 [nucl-th]].